

SRAD, Optical Flow and Primitive Prior Based Active Contours for Echocardiography

Ali K. Hamou and Mahmoud R. El-Sakka

Computer Science Department, The University of Western Ontario
London, Ontario, N6A 5B7, Canada
{ahamou,elsakka}@csd.uwo.ca

Abstract. Accurate delineation of object borders is highly desirable in echocardiography, especially the left ventricle. Among other model-based techniques, active contours (or snakes) provide a unique and powerful approach to image analysis. In this work, we propose the use of a novel external energy for a gradient vector flow (GVF) snake. This energy consists of optical flow estimates of heart sequences along with the use of a speckle reducing anisotropic diffusion (SRAD) operator. This energy provides more information to the active contour model garnering adequate results for noisy moving sequences. Furthermore, an automatic primitive shape prior algorithm was employed to further improve the results and regularity of the snake, when dealing with especially speckle laden echocardiographic images. Results were compared with expert-defined segmentations yielding better sensitivity, precision rate and overlap ratio than the standard GVF model.

Keywords: Image segmentation, active contours, gradient vector flow, optical flow, shape priors, curve fitting, echocardiography, speckle reducing anisotropic diffusion, instantaneous coefficient of variation.

1 Introduction

The assessment of cardiac function has been a major area of interest in the medical field. Normal heart function consists of pumping chambers (known as ventricles) which regulate the systemic and pulmonary circulation systems by delivering blood to the proper areas. Detection of non-normal heart function in the *left ventricle* (LV), for instance, can cause systolic dysfunction, being the reduction in the ability to contract, or diastolic dysfunction, being the inability to fill efficiently. Various heart structures may also fail causing cardiomyopathies, endangering the life of the host individual. Fortunately, many myopathies are treatable (with medication, implanted pacemakers, defibrillators, or ventricular assist devices) given early detection. Echocardiography, imaging the heart using ultrasound waves, facilitates the ability to do so.

The advent of real time ultrasonography provides the ability to image an entire LV and surrounding anatomy within one cardiac cycle (approximately one second). However, depending on the patient's 'photogenicity' (impacting factors include surrounding fatty tissues, calcifications, gender), these images are most likely marred by speckle artifacts. Many computer vision techniques attempt to reduce such speckle

noise by means of filtering [16] or incorporating the speckle effect directly into their algorithms [22]. Normally, these ultrasound images are analyzed for area and volume assessment by trapezoidal estimation. Such techniques introduce a large user bias into the calculations and are quite time consuming on the clinicians behalf. The advent of boundary detection techniques can help to automate this task. Boundary detection techniques are employed in order to segment the wanted regions for analyses on the heart structures, such as endocardial borders [4], stress and strain of the septum wall [17], and wall motility [1] to name a few.

Kass et al. [12] first proposed the original active contour model (commonly known as a snake or a deformable model). In their formulation, image segmentation was posed as an energy minimization problem.

Active contours treat the surface of an object as an elastic sheet that stretches and deforms when external and internal forces are applied to it. These models are physically-based, since their behaviour is designed to mimic the physical laws that govern real-world objects [5]. Since this approach relied on variational calculus to find a solution, time complexity was one of the main drawbacks of this original model. *Amini et al.* [2] proposed an algorithm for using dynamic programming, in order to incorporate soft and hard constraints into the formulation, improving time complexity and results. Further improvements to time complexity were proposed by *Williams et al.* [23], by using a greedy algorithm while incorporating a simple curvature approximation. Issues with large capture ranges and concavities are solved by other advances, which include inflation forces [6], probabilistic models [15], oriented particles [21], and gradient vector flows [24]. For the purposes of this study, focus will be placed on those advances best suited for echocardiographic images.

Since the LV represents one of the most important heart functions, many semi-automatic techniques attempt to segment this region from surrounding tissues [4][7][18]. Yet, no universally accepted standard exists for segmenting echocardiographic images.

Papademetris et al. [18] took advantage of a b-splines parameterized deformable model for segmenting cardiac regions. The external energy consisted of the standard intensity term and a texture-based *markov random field* (MRF) term. The MRF is based on a combination of gradient, regional and curvature data computed from the original image. Initial contours are manually placed for each 2D plane and are passed to a shape tracking algorithm. Displacements are probabilistically computed using a confidence measurement for the entire set. Final displacements are fed into an anisotropic linear elastic model which is computed vis-à-vis a Bayesian estimation framework. The manual placement of the contours makes this technique quite labour intensive.

Felix-Gonzalez et al. [7] proposed a segmentation technique for echocardiographic images using an *active surface model* (ASM). The ASM is made up of cubic splines and is based on a gradient descent procedure. When using gradient descent, the empirical setting of parameters is required based on the quality and types of images used. This makes this proposed technique extremely sensitive to its input. Furthermore, *Felix-Gonzalez et al.*'s work was only tested on two limited datasets.

Leung et al. [13] proposed the use of an *active appearance model* (AAM) and intensity based registration for segmenting multiple 2D image slices. An AAM uses all the information in an image region covered by the target object, rather than just that near modeled edges. An AAM involves the principal component analysis of the

various shapes and textures from several manually segmented 2D slices for training. The AAM makes use of the training set to converge the initial set mesh to the best textures on the image. However, this trained set required several manual segmentations of the 2D image slices to tune it to the medium being used.

The *gradient vector flow* (GVF) [24] snake was introduced as a modification to the original snake model in order to overcome the capture range and curve concavity issues. However, using the GVF snake directly on echocardiograms will not provide an adequate solution due to the complication of speckle noise and the existence of valves within the heart cavity, inhibiting a proper segmentation.

Zhou et al. [27] proposed the segmentation of MRI cardiac sequences using a generalized *fuzzy gradient vector flow* (FGVF) map along with a relative optical flow field. Optical flow measurements are computed on the cardiac sequence being considered and a *maximum a posteriori probability* (MAP) was used as a window for the movement of the curve. The use of optical flow with GVF provides promising results, however this technique is used exclusively on clear MRI data, and hence the presence of speckle noise on echocardiographic images would require modifications of this technique. Both GVF and optical flow measurements will be used in the proposed technique.

The proposed segmentation algorithm differs from previous works mainly in that it combines the benefits of multiple data sources within echocardiographic video cines. This includes the collection of motion data (helping to solve the static noise problem), localized detail data (helping to solve the inherent speckle noise problem), and structural data (helping to solve the occluded borders problem), which are represented by the optical flow module, the *speckle reducing anisotropic diffusion* (SRAD) edge map and the primitive priori knowledge module respectively.

The rest of this paper is organized as follows. In Section 2, the proposed scheme will be introduced. Results and discussion will be presented in Section 3, and Section 4 will contain conclusions.

2 System and Methods

In this study, we utilize and improve our previous preliminary works [8][9][10]. The proposed scheme will contain a fusion of knowledge about the image in order to improve the automation and inter-variable efficiency of left ventricular segmentation methods. The system will incorporate three distinct elements into the external energy of the active contour. These elements are SRAD measurements, optical flow estimates and priori knowledge measurements on contour points.

2.1 Parametric Active Contour Review

A snake is an energy minimization problem. Its energy is represented by two forces (internal energy, E_{in} , and external energy, E_{ex}) which work against each other. The total energy should converge to a local minimum – in the perfect case – at the desired boundary. The snake is defined as $v(s) = [x(s), y(s)]^T$, where s belongs to the interval $[0,1]$. Hence, the total energy to be minimized, E_{AC} , to give the best fit between a snake and a desired object shape is:

$$E_{AC} = \int_0^l E_{in}(v(s)) + E_{ex}(v(s)) ds \quad (1)$$

The internal energy decreases as the curve becomes smooth (by incorporating both elasticity and stiffness); whereas the external energy decreases as approaching the features of interest, such as image structures or edges.

The internal energy of the active contour formulation is further defined as:

$$E_{in}(v(s)) = \alpha(s) \left| \frac{dv(s)}{ds} \right|^2 + \beta(s) \left| \frac{d^2 v(s)}{ds^2} \right|^2 \quad (2)$$

where $\alpha(s)$ and $\beta(s)$ are weighting factors of elasticity and stiffness terms, respectively. The first order term makes the snake's surface act like a membrane. The weight $\alpha(s)$ controls the tension along the spine (stretching a balloon or elastic band). The second order term makes the snake act like a thin plate. The weight $\beta(s)$ controls the rigidity of the spine (bending a thin plate or wire).

A typical external energy formulation to identify edges for a given image, $I(x,y)$, is:

$$E_{ex}(x, y) = -|\nabla I(x, y)|^2 \quad (3)$$

where ∇ denotes the gradient operator. In the case of a noisier image the edges are further smoothed:

$$E_{ex}(x, y) = -|\nabla(G_\sigma(x, y) * I(x, y))|^2 \quad (4)$$

where $G_\sigma(x, y)$ is a two-dimensional Gaussian function with standard deviation σ , and $*$ denotes a convolution operator. Since the contour may get trapped by the noisy areas of the image, σ must be large enough to compensate for the image noise that would interfere with the active contour's capture range. The standard snake algorithm also suffers from poor capture range due to initialization and the inability to capture concavities. These problems are largely solved by the advent of the GVF snake [24].

The concavity problem exists since the gradient vectors in an image generally have large magnitudes only in the immediate vicinity of the boundary, and are nearly zero at points further away from the boundary. As such, the capture range of the snake will be quite small. In order to resolve this, the gradient map is extended to points away from boundaries using a computational diffusion process. The GVF field is used as an external energy in the active contour and is characterized by the vector field $z(x, y) = [u(x, y), v(x, y)]^T$ that minimizes the energy functional [24]:

$$E_{GVF} = \iint \mu (|\nabla u|^2 + |\nabla v|^2) + |\nabla f|^2 |z - \nabla f|^2 dx dy \quad (5)$$

where f is an edge map derived from the image, μ is the degree of smoothness of the field, u and v characterize the direction and strength of the field. Hence, when $|\nabla f|$ is small the energy will be dominated by the partial derivates, yielding a slow field. Alternatively, when $|\nabla f|$ is large, the latter term dominates and the function is minimized by setting $z = \nabla f$.

The external energy for the proposed scheme will be generated using a *virtual electric field* (VEF) [19] of f over the traditional GVF technique. Traditional GVF field

generation is performed by optimizing the cost function represented as the different partials shown in (5), which is quite a time consuming process. The VEF is defined by considering each edge pixel as a point charge within an electric field. This can be accomplished by convolving the edge map with the following two masks:

$$g_x(x, y) = \frac{-c \cdot x}{(x^2 + y^2)^{3/2}} \quad (6)$$

$$g_y(x, y) = \frac{-c \cdot y}{(x^2 + y^2)^{3/2}} \quad (7)$$

where $c = (4\pi\varepsilon)^{-1}$ and ε is sufficiently small constant. The resulting field yields a vector flow identical to a GVF field; given the masks are of sufficient size. A smaller mask size would ignore outlying edges that would have little impact on the interested features since their range is quite far. However, since echoardiographic images contain many features throughout the image, quantizing any part of the edge map is not an option.

According to Park *et al.* [19], an area of radius 32 around the feature should provide adequate flow vectors to accurately recreate a GVF field, without suffering from the high computational cost associated with vector flow generation. Fig. 1(b) shows an example of a vector flow field on the standard U-Image, shown in Fig. 1(a), using 65×65 masks generated from (6) and (7), which is identical to the original GVF field.

2.2 SRAD Measurements

Diffusion is a process that equalizes differing concentrations without creating or destroying an object's mass. Simple diffusion can be defined as

$$\frac{\partial p^t}{\partial t} = \operatorname{div}(D \cdot \nabla p^t) \quad (8)$$

where div is the divergence operator, D is the diffusivity tensor, and p refers to the diffused image at time point t . In Perona and Malik's anisotropic diffusion model [20], they define D for smoothing image data as

$$D = g(\|\nabla p^t\|) = \frac{1}{1 + \left(\frac{\|\nabla p^t\|}{\lambda}\right)^2} \quad (9)$$

where λ is the edge magnitude parameter. Hence, $g(\cdot)$ will yield low values (near zero) for gradient values much greater than λ inhibiting diffusion near edges. Using (9) as the diffusivity coefficient of (8), the model sharpens edges if their gradient value is larger than the edge magnitude parameter λ by inhibiting diffusion. In other words, $g(\cdot)$ acts as a means to standardize edge response across homogeneous regions and non-homogeneous regions.

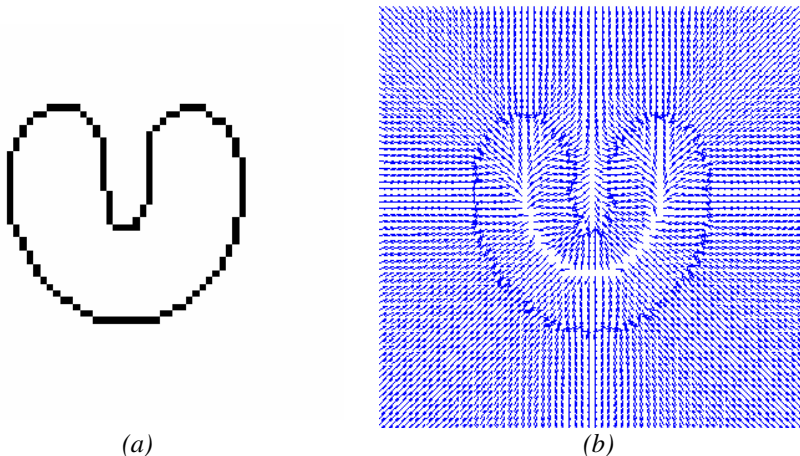


Fig. 1. Example of gradient vector forces; (a) standard U-Image, and (b) Gradient Vector Flow of U-Image

Yu et al. [25] introduced the *instantaneous coefficient of variation* (ICOV) as a noise-estimating operator. The ICOV operator is defined by

$$ICOV(p^t) = \frac{\sqrt{1/2 \cdot \|\nabla p^t\|^2 - 1/16 \cdot (\nabla^2 p^t)^2}}{(p^t + 1/4 \cdot \nabla^2 p^t)} \quad (10)$$

where ∇^2 is the Laplacian operator. By combining the anisotropic diffusion model with the ICOV operator, *Yu et al.* [25] yielded a partial differential equation called the *speckle reducing anisotropic diffusion (SRAD)*.

$$SRAD(p^t) = p^{t+\Delta t} = p^t + \frac{\Delta t}{|\eta|} \cdot \text{div}(g(ICOV(p^t)) \cdot \nabla p^t) \quad (11)$$

where, $|\eta|$ is the number of pixels in the neighbourhood of pixel x (usually taken to be equal four). *Yu et al.* [26] showed that using (11) provided better results at detecting real borders when faced with high levels of speckle noise.

Applying SRAD on the echocardiograms will help to reduce much of the speckle that impedes the accurate calculation of optical flow, which will be incorporated into the external energy. SRAD edge-maps will also be fed as the gradient estimates for the snake.

2.3 Optical Flow Estimates

Optical flow approximates the apparent motion of an object over a series of images (or time). The relationship between the optical flow in the image plane and the velocities of objects in the three dimensional world is not necessarily obvious [3]. For the sake of convenience, most optical flow techniques consider a particularly simple world where the apparent velocity of brightness patterns can be directly identified

with the movement of surfaces in the scene. This implies that objects maintaining structure but changing intensity would break this assumption.

Consider an image intensity, $I(x, y, t)$ at time t . Time, in this instance, implies that next frame in an image cine. Assuming that at a small distance away, and some time later the given intensity is:

$$I(x + \Delta x, y + \Delta y, t + \Delta t) = I(x, y, t) + \frac{\partial I}{\partial x} \Delta x + \frac{\partial I}{\partial y} \Delta y + \frac{\partial I}{\partial t} \Delta t + \text{higher order terms} \quad (12)$$

Given that the object started at position (x, y) at time t , and that it moved by a small distance of $(\Delta x, \Delta y)$ over a period of time Δt , the following assumption can be made:

$$I(x + \Delta x, y + \Delta y, t + \Delta t) = I(x, y, t) \quad (13)$$

The assumption in (13) would only be true if the intensity of our object is the same at time t and $t + \Delta t$. Furthermore, if our Δx , Δy and Δt are very small, our higher order terms would vanish, i.e.,

$$\frac{\partial I}{\partial x} \Delta x + \frac{\partial I}{\partial y} \Delta y + \frac{\partial I}{\partial t} \Delta t = 0 \quad (14)$$

Dividing (14) by Δt will yield:

$$-\frac{\partial I}{\partial t} = \frac{\partial I}{\partial x} \frac{\Delta x}{\Delta t} + \frac{\partial I}{\partial y} \frac{\Delta y}{\Delta t} \quad (15)$$

$$-I_t = \frac{\partial I}{\partial x} u + \frac{\partial I}{\partial y} v, \quad \text{where } u = \frac{\Delta x}{\Delta t} \text{ and } v = \frac{\Delta y}{\Delta t}. \quad (16)$$

Equation (16) is known as the optical flow constraint equation, where I_t at a particular pixel location, (x, y) , is how fast its intensity at this location is changing with respect to time, u and v are the spatial rates of change for any given pixel (i.e., how fast an intensity is moving across an image). However, effectively estimating the component of the flow (along with intensity values) cannot directly be solved in this form since it will yield one equation per pixel for every two unknowns, u and v . In order to do so, additional constraints must be applied to this equation.

Lucas-Kanade [14] and *Horn-Schunck* [11] introduced two common methods for solving this problem using partial derivatives. The former assumes that the flow field is locally smooth (for a given static window size) and then solves (16) by means of a least squares approximation technique. The latter uses a global regularization parameter which assumes that images consist of objects undergoing rigid motion, resulting in a smooth optical flow over a relatively large area. Fig. 2 depicts a visual representation of the optical flow of a simple Rubik's cube. Notice that the greyscale image has few shadows, helping to maintain consistency in the luminance of each pixel, hence yielding accurate results.

When dealing with noisy echocardiograms, a global regularization parameter will deal with the speckle better than the static window. This is due to the speckle noise remaining relatively static, lacking fluidity, throughout an image. Hence, the speckle

will be ‘filtered’, since the optical flow calculations will fail to realize it within the frames.

Optical flow magnitudes will be combined with the SRAD edge maps (see Section 2.5), in order to generate the external energy in (1) of the GVF snake. This will help to reduce artifacts due to static speckle noise, while also providing more information for the contour points to track (i.e., the movement of the tissue mass).

2.4 Primitive Shape Measurements on Contour Points

Since we are dealing with structures that have known shapes and sizes, and many real world models have been already measured, prior knowledge information can be directly used to increase the performance of a segmentation algorithm. Priors based on shape statistical models require modifications to the standard active contour model. An iterative solution can be incorporated directly into any optimization model by using the proposed framework.

Since it is desirable to incorporate shape priors without directly involving the user for training, automatic shape detection takes place on the set of discrete snake points, $v(s)$. This is achieved by first generating the least squares fit polynomial(s) of the current $v(s)$ points. For our left ventricle application, snake points were divided into an upper region and a lower region representing two separate third-order hyperbolulas, which will better suit the shape of the left ventricle during both systole and diastole, though any shape prior can be represented by means of simple primitives. Least squares fitting technique is utilized to estimate the two hyperbolulas coefficients. The axis separating the two regions is computed by taking the two-thirds upper and one-third lower bounds on all snake points and computing their division. This division can be tuned by shifting it upwards or downwards (either manually by the user or automatically by the system) in order to minimize the distance between the fitted hyperbolulas and snake points.

Priors are then generated by joining the fitted primitives to form one solid shape. Primitives are bounded by the furthest easterly and westerly points by the snake points, in order to prevent the possibility of a non-connecting shape.

Once priors have been generated, its GVF field is computed. This new field will replace the existing external energy of the GVF snake for this specific snake iteration. Fig. 3 portrays the process of generating a primitive prior for the left ventricle of the 4-chamber view image, where two intersecting hyperbolulas are used (default shape for our left ventricle application).

The fitting of a primitive shape (or a series of primitives as needed for the left ventricle) to the snake points, $v(s)$, will help compensate for the noise that inhibits the snake from migrating past a certain point. It will also help retract the snake towards the primitive prior when an occluded border exists; common in many echocardiographic images. The user can control the number of cycles between any two consecutive prior calculation cycles (prior step parameter). This allows for the increase or decrease in the inherent effect of the prior knowledge to the snake’s convergence cycle.

This primitive prior module is useful in the medical arena where the specialist or clinician has a clear understanding of the underlying structure being detected, such as a liver, an artery, or a heart. They can choose their desired primitive shape (or series of shapes) before curve evolution takes place.

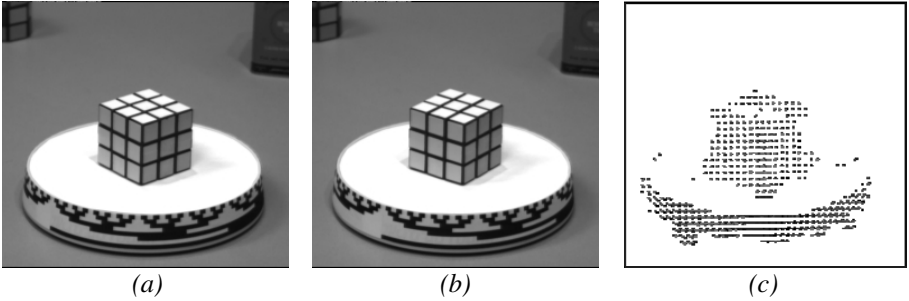


Fig. 2. An example of an optical flow field on a Rubik's cube rotated image; (a) cube at time t , (b) cube at time $t+\Delta t$, and (c) Optical flow of image (a) to (b) using Lucas-Kanade method (originally published in Barron *et al.* [3]).

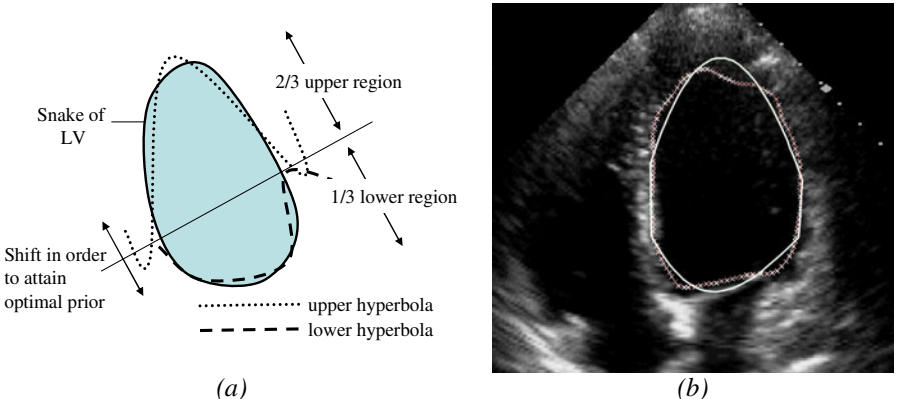


Fig. 3. Left ventricle primitive shape fitting; (a) primitive shape fitting algorithm using two hyperbolae, and (b) echocardiogram with segmentation overlay; solid line represents primitive whereas X-line represents active contour.

2.5 Fusion Characteristics

The proposed external energy is a fusion of SRAD gradient edge-map information and the optical flow estimates. Fig. 4 illustrates a top-level block diagram of the proposed system. It starts by calculating the SRAD edge map of the image cines (as explained in Section 2.2). The edge maps optical flows are then extracted (as explained in Section 2.3). The estimated optical flow is median filtered and are added to the SRAD image edge map following normalization. This result is used to generate the GVF for the snake's external energy. GVF snake evolution (as explained in Section 2.1) iterates to further minimize the energy function until a prior cycle condition is satisfied (as explained in Section 2.4), at which, the prior cycle is initiated. During the prior cycle, a GVF is generated from the desired primitive and a single optimization evolution of the snake is executed before returning to the original non-primitive snake iterations. This process is repeated until the snake is optimized and equilibrium is achieved.

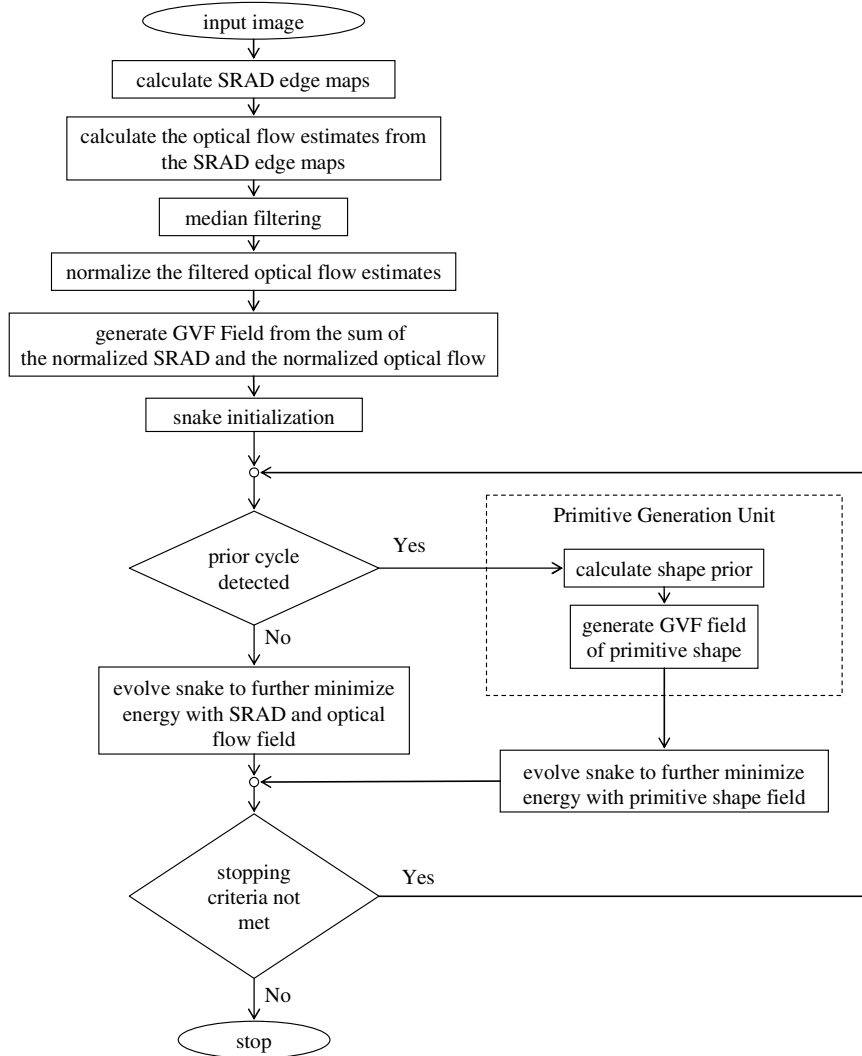


Fig. 4. Top level block diagram of proposed scheme

3 Results and Discussion

For this study, a series of B-mode echocardiogram cross-sectional videos of the heart have been used to investigate the proposed snake algorithm. These videos were acquired using a SONOS 5500 by Philips Medical System. The transducer frequency was set at 2.5 MHz in order to insure adequate penetration of tissue, while maintaining image quality with the existing speckle noise. Longitudinal views of the heart, which visualize the left ventricle, were acquired in order to verify the prior knowledge algorithm using more than one primitive shape.

The videos were parsed into image cines and each frame was considered with its direct neighbouring frame. Optical flow calculations for the edge map were completed using the Horn-Schunck technique with a regularization constraint of 0.2 in order to compensate for the general speckle throughout the US images. The initial contour placement was set to a small circle which was placed by the user within the left ventricle of the heart and the prior step parameter was set to 5 cycles.

Overall, experiments were run on eight complete cardiac cycles from different patients. The performance of the proposed system was measured by comparing 130 indexed segmented image cines from the eight cardiac cycles to the manually delineated segmentations by an expert radiologist, representing the gold standard used. Since the images at hand were mainly small-segmented foregrounds (left ventricular surface area) against vast backgrounds, the system performance would best be measured by means of its sensitivity, precision rate and overlap ratio. Let us consider the following metrics; a true positive pixel is a pixel that is considered part of the left ventricle by both of the proposed method and the gold standard. A false positive pixel is a pixel that is considered part of the left ventricle by the proposed method but it is not considered as such on the gold standard. A false negative pixel is a pixel that is not considered as part of the left ventricle by the proposed method, yet it is considered to be part of the ventricle according to the gold standard. The sensitivity is the percentage of the number of true positive pixels divided by the sum of the number of true positive pixels and false negative pixels. In other words, it classifies how well a binary classification test correctly identifies a condition. Precision rate is the percentage of the number of true positive pixels divided by the sum of the number of true positive pixels and false positive pixels. In other words, it classifies how accurate the results of the test when the results are positive. Overlap ratio is the percentage of the number of true positive pixels divided by the sum of the number of true positive pixels, false positive pixels and false negative pixels.

The sensitivity, precision rate and overlap ratio of the proposed system on the 130 segmented cines are shown in Table 1. This was generated by combining the total metric aggregates across all 130 cines, and calculating the sensitivity, precision rate and overlap ratio measures. Examination of Table 1 shows that the proposed technique outranks the standard GVF snake in all of the metrics shown.

Table 1. Sensitivity, precision rate and overlap ratio of the proposed system

	Sensitivity	Precision Rate	Overlap Ratio
Standard GVF Snake	90.4%	70.2%	65.3%
GVF Snake with SRAD	92.9%	77.4%	73.0%
Optical flow and priors			

An example of segmentation results is exhibited in Fig. 5, where Fig 5(b) reveals the SRAD contours used in the external energy of the proposed scheme, Fig(c) shows the expert manually traced delineation of the left ventricle, (d) shows the segmentation results when utilizing GVF only, and Fig 5(e) reveals the segmentation results when utilizing the proposed scheme. As seen in Fig(e), the shape priors improve regularity by allowing the snake to overcome various noise artifacts. This allows for proper delineation of the left ventricular endocardial lining. Furthermore,

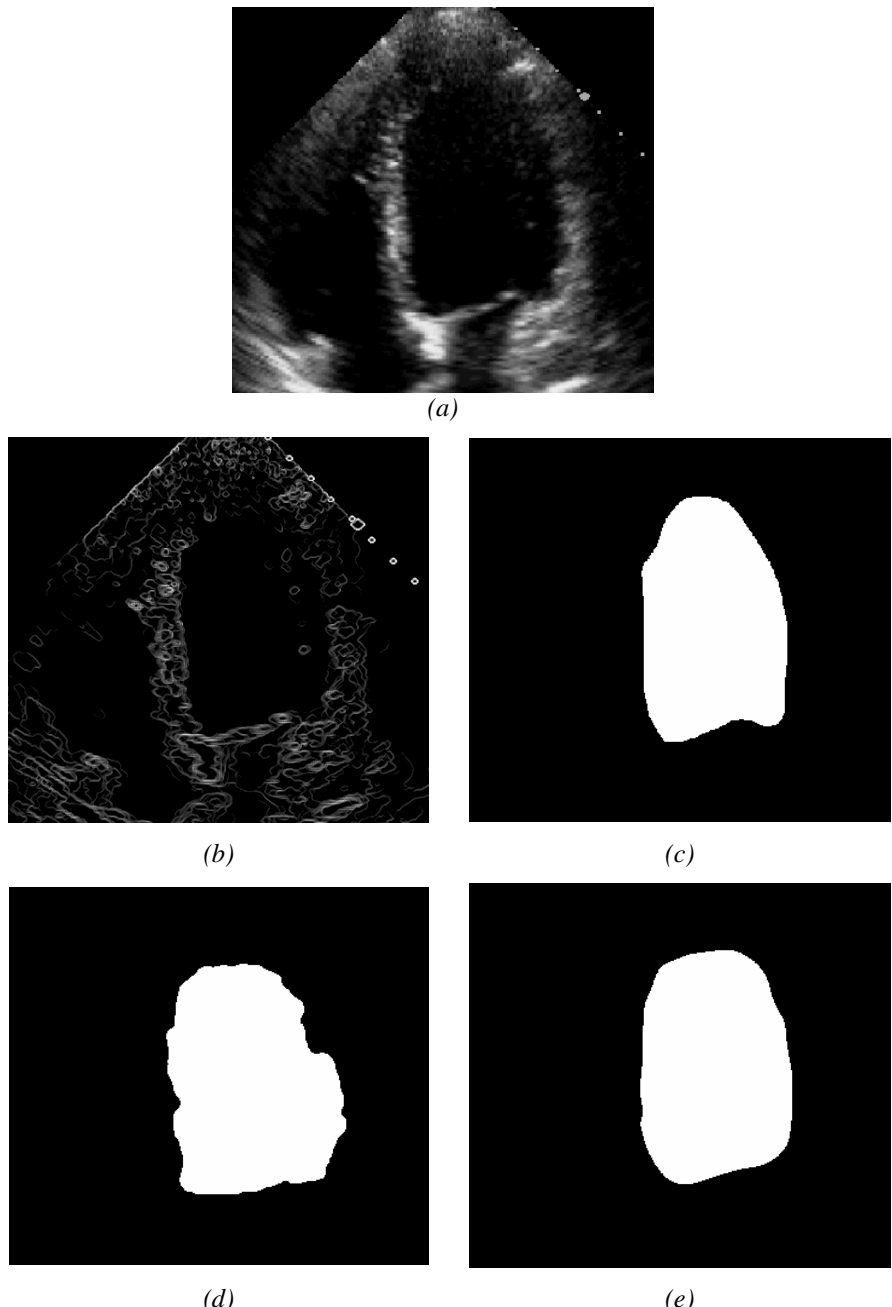


Fig. 5. Segmentation results; (a) LV echocardiogram, (b) SRAD diffusion of image (a), (c) manual expert delineation of image (a), (d) and (e) segmentations when utilizing GVF only and when utilizing the proposed scheme, respectively

the motion information (optical flow) is used as structural information in the external energy of the snake.

4 Conclusions

In this work, we have shown that the use of optical flow estimations and SRAD diffusion techniques perform well when integrated with a GVF active contour. This scheme helped alleviate the inherent difficulties in segmenting echocardiograms, such as considering speckle noise and contour bleeding. Furthermore, it strengthens the principle that tissue movement should be considered within segmentation techniques, where the data facilitates it.

Contour regularity and accuracy were further improved by using primitive shapes priors. The inherent difficulties in segmenting echocardiographic images, such as avoiding speckle noise and valve interference were also overcome by the primitive priors. Results were validated against a gold standard, which was manually segmented by a clinician and yielded stronger results than the standard GVF snake in sensitivity, precision rate and overlap ratios. Such segmentations would improve the calculation of various clinical measures by reducing the inconsistencies and variability between clinicians while simultaneously reducing the time for clinician interaction.

Acknowledgements. This research is partially funded by the Natural Sciences and Engineering Research Council of Canada (NSERC). This support is greatly appreciated.

References

1. Amini, A., Radeva, P., Elayyadi, M., Li, D.: Measurement of 3D motion of myocardial material points from explicit B-surface reconstruction of tagged MRI data. In: Wells, W.M., Colchester, A.C.F., Delp, S.L. (eds.) MICCAI 1998. LNCS, vol. 1496, pp. 110–118. Springer, Heidelberg (1998)
2. Amini, A., Weymouth, T., Jain, R.: Using dynamic programming for solving variational problems in vision. *IEEE Trans. on Pattern Analysis in Machine Intelligence* 12(9), 855–866 (1990)
3. Barron, J., Fleet, D., Beauchemin, D.: Performance of optical flow techniques. *Int. J. of Computer Vision* 12(1), 43–77 (1994)
4. Choy, M., Jin, J.: Morphological image analysis of left ventricular endocardial borders in 2D echocardiograms. In: SPIE Proceedings on Medical Imaging, vol. 2710, pp. 852–864 (1996)
5. Cohen, L.: On active contour models and balloons. *Computer Vision, Graphics, and Image Processing: Image Understanding* 53(2), 211–218 (1991)
6. Cohen, L., Cohen, I.: Finite-element methods for active contour models and balloons for 2-D and 3-D images. *IEEE Trans. on Pattern Analysis and Machine Intelligence* 15(11), 1131–1147 (1993)
7. Felix-Gonzalez, N., Valdes-Cristerna, R.: 3D echocardiographic segmentation using the mean-shift algorithm and an active surface model. In: Medical Imaging. SPIE, vol. 6144, pp. 147–151 (2006)

8. Hamou, A., El-Sakka, M.: An SRAD and optical flow based external energy for echocardiograms. In: Int. Conf. of Image Processing (2009)
9. Hamou, A., El-Sakka, M.: Active contours with Optical Flow and Primitive Shape Priors for echocardiographic Imagery. In: Int. Conf. of Imaging Theory and Applications, pp. 111–118 (2009)
10. Hamou, A., Osman, S., El-Sakka, M.: Carotid ultrasound segmentation using DP active contours. In: Kamel, M.S., Campilho, A. (eds.) ICIAR 2007. LNCS, vol. 4633, pp. 961–971. Springer, Heidelberg (2007)
11. Horn, B., Schunck, B.: Determining optical flow. Artificial Intelligence 17, 185–203 (1981)
12. Kass, M., Witkin, A., Terzopoulos, D.: Snakes: active contour models. Int. J. of Computer Vision 1(4), 321–331 (1987)
13. Leung, K., van Stralen, M., van Burken, G., Voormolen, M., Nemes, A., ten Cate, F., de Jong, N., van der Steen, A., Reiber, J., Bosch, J.: Sparse appearance model based registration of 3D ultrasound images. In: Yang, G.-Z., Jiang, T.-Z., Shen, D., Gu, L., Yang, J. (eds.) MIAR 2006. LNCS, vol. 4091, pp. 236–243. Springer, Heidelberg (2006)
14. Lucas, B., Kanade, T.: An iterative image registration technique with an application to stereo vision. In: Proceedings of Imaging Understanding Workshop, pp. 121–130 (1981)
15. Mallouche, H., de Guise, J., Goussard, Y.: Probabilistic model of multiple dynamic curve matching for a semitransparent scene. In: Vision Geometry IV, vol. 2573, pp. 148–157 (1995)
16. Mazumdar, B., Mediratta, A., Bhattacharyya, J., Banerjee, S.: A real time speckle noise cleaning filter for ultrasound images. In: IEEE Symposium on Computer-Based Medical Systems, pp. 341–346 (2006)
17. Montagnat, J., Delingette, H.: Space and time shape constrained deformable surfaces for 4D medical image segmentation. In: Delp, S.L., DiGoia, A.M., Jaramaz, B. (eds.) MICCAI 2000. LNCS, vol. 1935, pp. 196–205. Springer, Heidelberg (2000)
18. Papademetris, X., Sinusas, A., Dione, D., Duncan, J.: 3D cardiac deformation from ultrasound images. In: Taylor, C., Colchester, A. (eds.) MICCAI 1999. LNCS, vol. 1679, pp. 420–429. Springer, Heidelberg (1999)
19. Park, H., Chung, M.: A new external force for active contour model: virtual electric field. In: Int. Conf. on Visualization, Imaging and Image Processing, pp. 103–106 (2002)
20. Perona, P., Malik, J.: Scale space and edge detection using anisotropic diffusion. IEEE Trans. Pattern Analysis Machine Intelligence 12(7), 629–639 (1990)
21. Szeliski, R., Tonnesen, D.: Surface modeling with oriented particle systems. SIGGRAPH: Computer Graphics 26(2), 185–194 (1992)
22. Tauber, C., Batatia, H., Ayache, A.: Robust B-spline snakes for ultrasound image segmentation. J. of Signal Processing Systems 54(1), 159–169 (2009)
23. Williams, D., Shah, M.: A fast algorithm for active contours and curvature estimation. Computer Vision Graphics and Image Processing: Image Understanding 55(1), 14–26 (1992)
24. Xu, C., Prince, J.: Snakes, shapes, and gradient vector flow. IEEE Trans. on Image Processing 7(3), 359–369 (1998)
25. Yu, Y., Acton, S.: Speckle reducing anisotropic diffusion. IEEE Trans. on Image Processing 11(11), 1260–1270 (2002)
26. Yu, Y., Acton, S.: Edge detection in ultrasound imagery using the instantaneous coefficient of variation. IEEE Trans. on Image Processing 13(12), 1640–1655 (2004)
27. Zhou, S., Liangbin, C.W.: A new method for robust contour tracking in cardiac image sequences. In: IEEE Int. Symposium on Biomedical Imaging: Nano to Macro, vol. 1, pp. 181–184 (2004)